AGU PUBLICATIONS

JGR

Journal of Geophysical Research: Atmospheres

RESEARCH ARTICLE

10.1002/2014JD022170

Key Points:
- The frequency of SSWs depends as much on radiative as on orographic forcing
- Damping rates in low and high latitudes have similar effects on SSW frequency
- Only polar cap zonal wind shows strong correlation to SSW frequency

Correspondence to:
M. Jucker,
mjucker@nyu.edu

Citation:
Jucker, M., S. Fueglistaler, and G. K. Vallis (2014), Stratospheric sudden warmings in an idealized GCM, *J. Geophys. Res. Atmos.*, *119*, 11,054–11,064, doi:10.1002/2014JD022170.

Received 16 JUN 2014
Accepted 27 AUG 2014
Accepted article online 30 AUG 2014
Published online 6 OCT 2014
Corrected 18 Nov 2014

This article was corrected on 18 NOV 2014. See the end of the full text for details.

Stratospheric sudden warmings in an idealized GCM

M. Jucker[1,2], S. Fueglistaler[1,2], and G. K. Vallis[3]

[1]Program in Atmospheric and Oceanic Sciences, Princeton University, Princeton, New Jersey, USA, [2]Now at Courant Institute of Mathematical Sciences, New York University, New York, New York, USA, [3]Mathematics, and Physical Science, College of Engineering, Exeter University, Exeter, UK

Abstract An idealized general circulation model (GCM) with an analytically described Newtonian cooling term is employed to study the occurrence rate of sudden stratospheric warmings (SSWs) over a wide range of parameters. In particular, the sensitivity of the SSW occurrence rates to orographic forcing and both relaxation temperature and damping rate is evaluated. The stronger the orographic forcing and the weaker the radiative forcing (in both temperature and damping rate), the higher the SSW frequency. The separate effects of the damping rates at low and high latitudes are somewhat more complex. Generally, lower damping rates result in higher SSW frequency. However, if the low- and high-latitude damping rates are not the same, SSW frequency tends to be most sensitive to a fractional change in the lower of the two damping rates. In addition, the effect of the damping rates on the stratospheric residual circulation is investigated. It is found that higher high-latitude damping rate results in deeper but narrower circulation, whereas higher low-latitude damping rates cause strengthening of the stream function in the tropical midstratosphere to upper stratosphere. Finally, the relation between easily measured and compared climatological fields and the SSW occurrence rate is determined. The average stratospheric polar zonal mean zonal wind shows a strong anticorrelation with the SSW frequency. In the troposphere, there is a high correlation between the meridional temperature gradient and SSW frequency, suggesting that the strength of synoptic activity in the troposphere may be an important influence on SSW occurrence.

1. Introduction

Sudden stratospheric warmings (SSWs) are not only events with dramatic change in zonal wind and temperature in the stratosphere but they may also play a role in stratosphere-troposphere coupling [*Baldwin and Dunkerton*, 2001] and in the seasonal variability of the troposphere [*Holton et al.*, 1995; *Baldwin et al.*, 2003; *Kodera*, 2006; *Charlton and Polvani*, 2007; *Mitchell et al.*, 2013; *Sigmond et al.*, 2013]. General circulation models (GCMs) have long been recognized as indispensable for studying the underlying dynamical and radiative processes. *Miyakoda et al.* [1970] attempted to reconstruct a specific SSW with an early GCM and found that upward propagating large-scale perturbations from the troposphere provide the necessary eddy kinetic energy in the stratosphere. *Kouker and Brasseur* [1986] constructed an idealized model of a major warming based on the primitive equations and with wave-one topographic forcing, and find considerable irreversible mixing between air masses originating from the subtropics and high latitudes. *Yoden et al.* [1999] constructed composites of SSW evolution from more comprehensive GCM simulations, run in perpetual January configuration, in order to obtain better statistics with a higher number of events than in the observational archives.

However, even more recent attempts to fully understand SSWs with more sophisticated models have not yet provided conclusive theories of the circumstances under which SSWs develop or are suppressed; and if they occur, it is not clear what determines whether or not a given sudden warming will influence the tropospheric circulation [*Limpasuvan et al.*, 2004; *Nakagawa and Yamazaki*, 2006; *Kodera*, 2006; *Charlton and Polvani*, 2007; *Sigmond et al.*, 2013].

In this work, we employ an idealized general circulation model to study the effects of orographic and radiative forcing on the occurrence rate of SSWs, extending earlier work by *Polvani and Kushner* [2002], *Kushner and Polvani* [2004], *Gerber and Polvani* [2009], and *Jucker et al.* [2013]. In particular, we will show that troposphere-stratosphere coupling in terms of SSW frequency is as sensitive to the relaxation time scale as it is to orographic forcing and relaxation temperature.

Our primitive equation model is based on Geophysical Fluid Dynamics Laboratory's (GFDL) dry dynamical core and forced by Newtonian cooling. The relaxation temperature and damping rate (or relaxation time

scale) stand for a linearization of all diabatic processes in the real atmosphere. Our model is based on the radiatively determined base state of *Jucker et al.* [2013] but with prescribed relaxation temperature and time scale in analytical form. This allows us to study the sensitivity of stratosphere-troposphere coupling as a function of a few chosen model parameters.

After describing the model setup in more detail in section 2, we investigate the effect of the strength of orographic forcing and radiative forcing in the base state temperature profile on SSW frequency in Section 3.1. As expected, and in broad agreement with earlier studies [e.g., *Gerber and Polvani*, 2009], we find that stronger orographic forcing and weaker polar vortex in the relaxation temperature result in higher SSW frequency. It is this result that explains why sudden warmings are frequent in the Northern Hemisphere winter (strong orographic forcing and weak polar vortex) but rare in the Southern Hemisphere (weak orographic forcing and strong polar vortex). Following this, in section 3.2, we investigate the role of the thermodynamic damping rates on SSWs, and on the residual (Brewer–Dobson) circulation in section 4. In particular, we differentiate between the effects of the damping rates at low and high latitudes. Finally, in section 5, we address the question of whether or not the SSW frequency can be inferred from observable variables instead of model specific parameters as the latter cannot be directly observed. We show that the only quantity showing strong (anti)correlation throughout the stratosphere with SSW frequency is the average near-polar zonal mean zonal wind, whereas in the troposphere the meridional temperature gradient shows highest correlation with SSW frequency.

2. Model Setup

2.1. Idealized Forcing

The model used for this work is based on GFDL's spectral dynamical core, with T42 horizontal resolution and 40 vertical levels extending from the surface to about 0.01 hPa. All parameters not discussed below are described in *Jucker et al.* [2013]. In the latter paper, we described an idealized model for studying the stratosphere that included orographic forcing and a seasonally dependent Newtonian thermal relaxation of the form

$$Q = -\frac{T - T_e(\varphi, p, t)}{\tau(\varphi, p, t)}, \tag{1}$$

where Q is the diabatic heating rate, T the temperature, T_e is the relaxation temperature, and τ the relaxation time scale. Latitude, pressure, and time are denoted by φ, p, and t, respectively. The parameters T_e and τ were previously numerical fields. In this section we present analytic approximations for these parameters that, as far as possible, preserve the behavior of the original scheme.

The exact form of the analytic profiles is given in Appendix A, with the relaxation temperature given in section A1 and the relaxation time given in section A2. In addition, any code that differs from GFDL's original model is provided online at https://github.com/mjucker/JFV-strat. The profiles introduce a number of independent parameters, which are given with their default values (based on typical January/July configurations) in Tables A1 and A2.

In terms of T_e, these parameters determine the amplitudes of the polar vortex for the Northern and Southern Hemisphere winters and the respective summer hemisphere. The most important parameter for this study is the polar vortex amplitude, A^1_{NH}, which gives the difference in T_e at the winter pole compared to equinox conditions. For instance, $A^1_{\mathrm{NH}} = 10$ K means that over the North Pole, T_e is 10 K colder at 1 hPa than equinox conditions.

In terms of τ, the parameters describe the equator-to-pole difference in τ, with possible north-south asymmetry and time dependence. In particular, τ_p gives the value of the relaxation time at high latitudes and 100 hPa. Meridional dependence is included in form of a Gaussian centered at the equator, with the relaxation time at the equator and 100 hPa given by the parameter τ_t. Thus, setting $\tau_t = 40$ days and $\tau_p = 20$ days results in a relaxation time of 40 days over the equator smoothly changing to 20 days over high latitudes. The width of the Gaussian can be varied and is set to 30° in all of our simulations (see Figure A1 for an example profile).

We note that in our formulation, both T_e and τ can be functions of latitude, pressure, and time. While we repeat experiments with varying polar temperatures and orographic forcing for comparison with previously published results, the main focus of this work is on experiments with varying relaxation time scale. With our

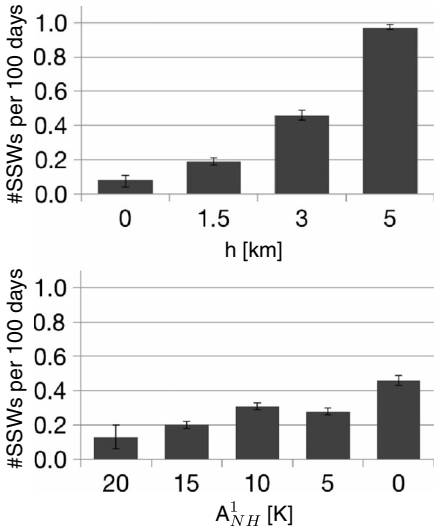

Figure 1. (top) A bar chart of SSW frequency versus orographic forcing (given in terms of mountain height h) and (bottom) the parameter A^1_{NH} determining the polar vortex strength. The polar vortex is stronger for higher A^1_{NH} and so gets weaker from left to right. The stronger the orographic forcing and the weaker the polar vortex, the higher the SSW frequency.

analytical description, the latter can be varied independently at low (τ_t) and high latitudes (τ_p). One motivation for this is to be able to quantify the effects of differences between distinct numerical model setups described in the literature. Indeed, many authors have emphasized the importance of latitudinal gradients in the relaxation time [e.g., *Kiehl and Solomon*, 1986; *Newman and Rosenfield*, 1997], but only few idealized studies of SSWs address this issue. By varying τ_t and τ_p independently, we can either increase or decrease the meridional gradient of the relaxation time and show how this impacts the occurrence rate of sudden warmings. In addition, there is a wide range of values for radiative damping rates in the literature, with values of 5 to over 100 days [*Dickinson*, 1973; *Fels*, 1982; *Ramanathan et al.*, 1983; *Ghazi et al.*, 1985; *Kiehl and Solomon*, 1986; *Newman and Rosenfield*, 1997; *Hartmann et al.*, 2001; *Charlton-Perez and O'Neill*, 2010; *Hitchcock et al.*, 2013]. Studies that vary τ in the stratosphere usually do not differentiate between high and low latitudes [e.g., *Charlton-Perez and O'Neill*, 2010; *Hitchcock et al.*, 2013]. In contrast, *Newman and Rosenfield* [1997] show that the polar damping rates have a seasonal cycle of between 60 and 10 days at 100 hPa, whereas the tropical damping rates show almost no seasonal cycle, indicating that the relaxation times in those two regions should be treated in a different manner. Furthermore, another motivation for varying τ is that depending on its value, perturbations with different vertical scales are damped more or less effectively [*Fels*, 1982; *Hartmann et al.*, 2001]. Finally, in a simple model with a forcing in the form of equation (1), one can obtain similar climatologies in temperature and zonal wind with different (T_e, τ) pairs, even for conceptually different reasons. For instance, we can increase the strength of the polar vortex by cooling T_e while keeping τ constant, mimicking radiative effects. We can generate the same effect by decreasing the high-latitude relaxation time τ_p and forcing the temperature closer to T_e, but in this case the wave damping properties have been changed.

2.2. Simulation Setups

In the next section, we will apply the analytical setup described in detail in Appendix A to the study of SSW frequency as a function of parameter space. All simulations assume perpetual Northern Hemisphere winter. Setups are different in the strength of radiative forcing in the stratosphere only, with warmer/colder polar vortex in T_e and weaker/stronger damping in the tropics, high latitudes, or globally. The tropospheric T_e/τ values are the same for all simulations, but surface forcing of planetary waves is varied with different topography heights and wave numbers. All of these parameters are independently adjustable. As a result, our simulations comprise a strong polar vortex without orographic forcing, similar to Earth's Southern Hemisphere, a weak polar vortex with orographic forcing, similar to Earth's Northern Hemisphere, and various states in between, which could be likened to early, deep, or late Northern or Southern Hemisphere winters in the real atmosphere.

The differences in model setups for our simulations are summarized in Table 1. All parameters not mentioned in the latter table assume their default values given in Tables A1 and A2. The climatological day of the year is set to $d = 0$ to allow for easier control of the polar vortex strength; with this choice $D(\varphi \geq 0, d) = 1$ in equation (A12). In addition, we choose the T_e amplitude at 100 hPa to be zero, i.e., $A^0_{\mathrm{NH}} = 0$ K, as we expect SSWs to be most numerous with a weaker polar vortex.

Orographic forcing is included, following *Gerber and Polvani* [2009], with sinusoidal wave-two topography in the Northern Hemisphere, with the amplitude set to $h = 3$ km unless stated otherwise. The seasonal cycle in the troposphere is fixed at a standard value of $\epsilon_{\mathrm{SH}} = 10$ K in the Southern Hemisphere and an enhanced value of $\epsilon_{\mathrm{NH}} = 40$ K in the Northern Hemisphere, in accordance with the previous findings in *Jucker et al.* [2013].

Table 1. Parameter Settings for All Setups[a]

Sim	h (km)	A^1_{NH} (K)	τ_t(d)	τ_p(d)	#SSWs
1	0	0	40	20	4
2	1.5	0	40	20	23
3	3	0	40	20	50
4	5	0	40	20	107
5	3	20	40	20	14
6	3	15	40	20	24
7	3	10	40	20	31
8	3	5	40	20	35
9	3	0	30	20	25
10	3	0	20	20	7
11	3	0	30	30	59
12	3	0	30	40	83
13	3	0	20	30	45
14	3	0	20	40	74
15	3	0	40	30	65
16	3	0	40	40	69

[a]The last column gives the number of SSWs for each simulation. Note that for these perpetual winter runs, none of the parameters depends on time, and we set $\tau_p^S = \tau_p^N \equiv \tau_p$.

We let the model spin up for 2000 days and then perform our analysis on the following 10,000 days. Table 1 shows the values of parameters we are varying for our different simulations. The last column gives the total number of SSWs for the last 10,000 days of each simulation. We apply the criterion that the zonal mean zonal wind reverses at 10 hPa and 60°N, as in, e.g. *Polvani and Waugh* [2004], *Charlton and Polvani* [2007], and *Gómez-Escolar et al.* [2012], and treat two occurrences as distinct if they are separated by at least 20 days.

3. SSW Frequency Versus Forcing Parameters

3.1. Orographic Forcing and Stratospheric Relaxation Temperature

As a zeroth order approximation, one may expect that colder and stronger polar vortices would allow fewer SSWs because a greater disruption is needed for a vortex break. Similarly, stronger orographic forcing can be expected to increase SSW frequency, other parameters held constant, and these expectations were substantiated by *Gerber and Polvani* [2009]. We confirm these general findings in Figure 1, where we plot the SSW frequency as a function of topography height h and T_e amplitude A^1_{NH} for simulations 1–8 in Table 1. In Figures 1 and 2, we determine the frequency of SSWs as given by the linear regression of number of SSWs detected onto integration days of the simulation. The error bars denote the range of 95% confidence interval of the regression coefficient. Clearly, stronger orographic forcing (larger h) enhances the occurrence rate of SSWs essentially because stronger orography enhances the planetary wave activity that can propagate into the stratosphere and cause sudden warmings. When varying the stratospheric background temperature gradient, one may force a stronger polar vortex (by increasing the value of A^1_{NH}). As a result, more and/or stronger large-scale wave breaking (Eliassen-Palm (EP) flux divergence) is needed for a complete reversal of the zonal mean zonal wind, and the EP flux itself is diverted by changing the zonal wind structure. The effect of decreasing the polar night relaxation temperature through A^1_{NH} is then a decrease in SSW frequency, with a maximum for the weakest polar vortex ($A^1_{NH} = 0$). These results may be regarded as a test of our new formulation. In addition, note that simulation 3 shows a SSW occurrence rate of 1/200 days, which is similar to Earth's Northern Hemisphere [*Charlton and Polvani*, 2007; *Gerber et al.*, 2012].

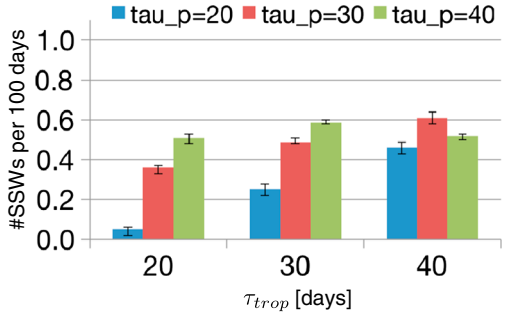

Figure 2. Frequency of sudden stratospheric warmings (SSWs) as a function of the parameters τ_t (i.e., τ_{trop}) and τ_p in (A16), i.e., the relaxation time at low and high latitudes at 100 hPa, respectively. Generally, the longer any relaxation time, the more SSWs occur. See text for more detailed discussion.

3.2. Effect of Relaxation Times

In this section, we extend previous SSW frequency studies and perform a parameter scan of radiative relaxation time scales. The values for all parameters different from their default values for these additional simulations are given in lines 9–16 of Table 1.

SSW frequency: We present here the results for varying the relaxation times at low and high latitudes independently, with values of 20, 30, and 40 days for each. We have also run simulations with a very short value of 10 days, both at low and high latitudes. However, the model produced such low numbers of SSWs during the 10,000 day runs (<10 SSWs) that these simulations do not add statistically meaningful

information to this section. Therefore, we do not show these simulations here. Figure 2 summarizes the results for all combinations of relaxation times from 20 to 40 days.

In general, longer-relaxation times result in more SSWs, and the SSW frequency is somewhat more sensitive to the value of the longer-relaxation time if $\tau_p \neq \tau_t$. The difference between different values of τ_p for any given τ_t (difference between different colors in Figure 2) scales inversely with τ_t, i.e., the longer the low-latitude relaxation time (the smaller the damping rate), the weaker the influence of the high-latitude relaxation time τ_p on the SSW frequency. A similar result holds for the opposite case. Given a certain value for τ_p (compare columns of same color in Figure 2), the difference in SSW frequency between two values of τ_t becomes smaller when increasing τ_p: The slope of the frequency $F(\tau_t, \tau_p = 20\,\mathrm{d})$ (blue columns) is steeper than the slope of $F(\tau_t, \tau_p = 30\,\mathrm{d})$ (red columns), and the slope of $F(\tau_t, \tau_p = 40\,\mathrm{d})$ (green columns) is essentially zero. Thus, if either τ_t or τ_p is fixed to a value that is large enough, the exact value of the other, τ_p or τ_t, is not crucial in terms of SSW frequency. However, the inverse is true as well: If either τ_t or τ_p is fixed to a value that is short enough, the value of the other, τ_p or τ_t, is very important in terms of SSW frequency. It is then interesting to note that the (τ_t, τ_p) pair closest to Northern Hemisphere variability of about one SSW every 200 days matches well with the radiatively found values of $(\tau_t = 40, \tau_p = 20)$ days [*Jucker et al.*, 2013]. Therefore, fixing τ_t to the most realistic value of 40 days, the value for τ_p can be chosen remarkably freely without large impact on SSW frequency (1/200 days for $\tau_p = 20$ d versus 1/140 days for $\tau_p = 40$ d). On the other hand, fixing τ_p to the most realistic value of 20 days, the value for τ_t is quite important, with SSW frequencies of 1/200 days for $\tau_t = 40$ d and 1/1430 days for $\tau_t = 20$ d. Thus, in the setup that is most similar to the real atmosphere ($\tau_t = 40$, $\tau_p = 20$ days), the exact value of the damping rate at low latitudes is more important than the exact value of the damping rate at high latitudes.

4. Effects of Damping Rate on Residual Circulation

Varying the extratropical damping rate can have two distinct effects on stratospheric dynamics, both impacting the occurrence rate of SSWs. One is local, where due to a long (short) relaxation time, the restoring force in the Newtonian cooling term becomes weak (strong); and thus, dynamics can push the system further from equilibrium (for same Q, $T - T_e$ scales with τ in equation (1)). From this mechanism, the form of T_e is defining the structure of the stratosphere, and τ regulates how far the dynamics can push the temperature away from T_e locally. We then expect more SSWs for large values of τ_p, the high-latitude relaxation time, which is what we see in Figure 2.

A second, more subtle way to influence stratospheric dynamics and SSW frequency is nonlocal through the residual meridional overturning circulation. As dynamics can (cannot) push the stratosphere far from the relaxation setup for long (short) relaxation times, the waveguide properties of the stratosphere change due to different zonal wind structures. With this, the Eliassen-Palm fluxes and therefore also the residual circulation change with changing τ_t and/or τ_p. This indirect effect is what we are concerned with in this section, as it not only impacts the frequency of SSWs but also chemical tracer distribution (such as ozone and water vapor), age of air, etc. through the regulation of the residual circulation.

To explore this, Figure 3 compares the residual stream functions of short versus long-extratropical relaxation times for given tropical relaxation time (top row) and short versus long-tropical relaxation times for given extratropical relaxation time (bottom row).

Negative (blue) values indicate that the circulation is weaker for stronger damping than for weaker damping, and positive (red) values indicate stronger circulation for weaker damping. It is helpful to recall from Table 1 or Figure 2 that, in general, longer-relaxation times translate into more SSWs.

Downward control would suggest that the generally weaker lower stratospheric circulation for shorter τ shown in Figure 3 means that less EP flux reaches the stratosphere. This can be expected to some extent, as upward propagating perturbations will be damped earlier when damping is stronger, but it confirms a nonlocal contribution to the general tendency for more SSWs at longer τ due to stronger circulation.

In addition to being weaker, the stream function is also narrower in latitude and deeper in altitude if the damping is stronger. This can be seen through the minima at low and high latitudes and the positive values in the upper stratosphere. Although the narrowing is strongest where the damping is modified (upwelling branch if τ_t is modified, downwelling branch if τ_p is modified), the strong symmetry around the midlatitudes suggests another nonlocal effect of localized damping modification: As less upwelling (downwelling)

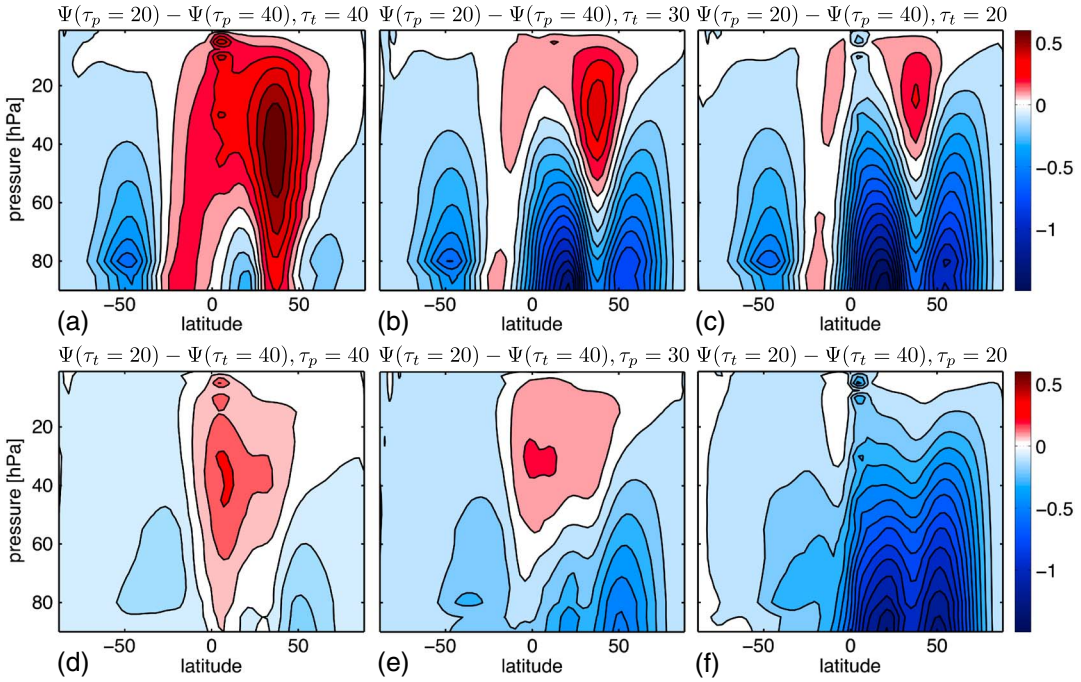

Figure 3. Difference of residual stream functions with short and long relaxation times. (a–c) Difference in stream function between integrations with $\tau_p = 20$ d and $\tau_p = 40$ d with τ_t having values 40, 30, and 20 days as labeled. (d–f) Difference in stream function between integrations with $\tau_t = 20$ d and $\tau_t = 40$ d with τ_p having values 40, 30, and 20 days as labeled. Contours denote intervals of 0.1×10^9 kg/s, and the color bars are in units of 1×10^9 kg/s. Red (blue) values denote a generally stronger (weaker) circulation.

in low (high) latitudes due to locally stronger damping restricts the mass flow into (from) the upper stratosphere, there must be less downwelling (upwelling) in high (low) latitudes due to mass conservation. In both Figures 3a–3c and Figures 3d–3f, the difference in lower stratospheric residual circulation becomes larger for smaller τ_p, accounting for the larger differences in SSW frequency in Figure 2 when decreasing τ_p (compare columns of same color).

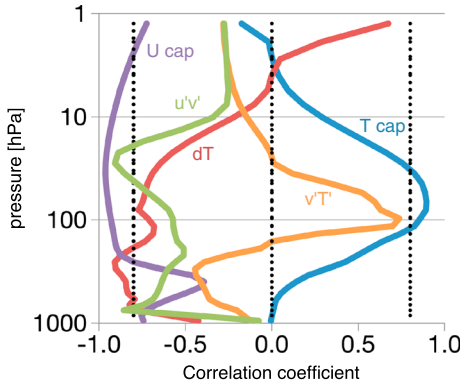

Figure 4. Correlation coefficients (R^2, negative for anticorrelations) from linear regression of various fields onto SSW frequency. The fields are the zonal and time mean mean zonal wind ("U cap," purple) and temperature ("T cap," blue) polar cap averages (60–90°N); midlatitude (40–60°N) minus polar cap temperatures ("dT," red); and extratropical (20–90°N) eddy heat flux ($v'T'$, orange) and momentum flux ($u'v'$, green) onto SSW frequency.

The stronger circulation in the upper midlatitude to low-latitude stratosphere with stronger damping seems counterintuitive and must be explained with changes in the refractive index as the zonal wind structure adjusts to different forcing. As a result, EP flux can propagate further into the upper stratosphere and mesosphere and drive stronger upper stratospheric circulation.

5. SSW Frequency Versus Dynamic Variables

We now turn to analyzing the relation between SSWs and observables such as zonal wind, temperature, or eddy heat flux. Taking all 16 simulations performed in this work (except the $h = 5$ km case, which is an outlier), we have compared regression coefficients between the SSW frequency and climatological (i.e., time mean) zonal means of dynamic variables such as zonal wind and temperature, or easily derived quantities such as eddy heat fluxes at different latitudes and heights. Figure 4 shows the correlation coefficients between the SSW frequency and the polar cap (cosine latitude weighted average from 60°N to 90°N) zonal mean zonal wind (purple) and

Table 2. R^2 Values for Correlations Between SSW Frequency and Climatological Variables, as in Figure 4

Variable	Highest R^2	at Level	R^2 at 10 hPa
$\overline{u}$ cap	0.96	36 hPa	0.92
$\overline{T}$ cap	0.89	66 hPa	0.29
$\Delta\overline{T}$	0.91	258 hPa	0.22
$\overline{v'T'}$	0.74	97 hPa	0.14
$\overline{u'v'}$	0.91	28 hPa	0.34

temperature (blue), the difference between the midlatitude (40°N to 60°N) and the polar cap temperature (red), and the extratropical (20°N to 90°N) eddy heat flux (orange) and momentum flux (green). For easier reading, lines have been added to the ±0.8 and 0.0 values of the correlation coefficient.

The strongest correlation throughout the stratosphere can be found for the polar zonal wind (purple), which has (anticorrelated) R^2 values of 0.8 and more above about 250 hPa almost all the way to 1 hPa, with the highest correlation of 0.96 at 36 hPa: With stronger zonally averaged climatological zonal wind, SSWs are less likely. This is also the only variable that shows strong correlation with SSW frequency at 10 hPa (see Table 2), which for historical reasons is the pressure level most often used to diagnose SSWs. We note that for these correlation studies, 10 hPa does not represent any special level. Indeed, 20–40 hPa seems more important (in agreement with *Gómez-Escolar et al.* [2012]), where the meridional momentum flux correlation shows a distinct peak. It is interesting to note that the only variable with strong (anti) correlation to SSW frequency in the troposphere is the temperature difference between the polar cap and the midlatitudes (red). We have tried different meridional regions for defining the low to high-latitude temperature difference, and the choice presented here (40 to 60°N versus 60 to 90°N) has the strongest correlations for the troposphere and lower stratosphere. The polar cap temperature correlates strongly to the SSW frequency in the lower to midstratosphere, but not elsewhere. The correlation of the eddy heat flux to SSW frequency has a clear peak around the 100 hPa level, where R^2 reaches about 0.74. Similarly, the eddy momentum flux $\overline{u'v'}$ (green) has a localized peak anticorrelation around 30 hPa, around the height at which $\overline{v'T'}$ switches from correlation to anticorrelation. We note that even for the highest-SSW frequencies measured in our simulations, eddy heat and momentum flux climatologies are not dominated by sudden warming events: Those events are very short compared to the total integration time; and for every positive burst before/during an event, there is a negative anomaly during recovery. Therefore, the rather strong correlations between eddy fluxes and SSW frequency (although localized) might hint at the idea of a preconditioning of the atmosphere with elevated eddy heat flux strength facilitating the occurrence of a strong SSW causing burst [*Limpasuvan et al.*, 2004]. In that picture, the weak climatological zonal wind would be caused by constantly strong deceleration due to enhanced EP flux divergence. As the cause and effect is not clear from these climatological plots, it might also mean that for weak (in terms of zonal wind) polar vortices, more perturbations can propagate high into the stratosphere (less reflection, but still positive zonal wind on average), increasing the probability for the occurrence of a SSW. In addition, our results seem to indicate that if EP fluxes reach altitudes higher than about 30 hPa on average, there are fewer SSWs than if they dissipate below that level, as the vertical component of the EP flux, the eddy heat flux, changes sign from positive to negative correlation around 30 hPa (Figure 4, orange line).

6. Summary and Conclusions

We have employed an idealized GCM to study the relationship between the occurrence rate (or frequency) of sudden stratospheric warmings (SSWs) and the form of radiative forcing in the stratosphere and surface orographic forcing. Our numerical model is based on a Newtonian cooling scheme with analytically described relaxation temperature and time based on that of *Jucker et al.* [2013], which was constructed with detailed radiative perturbation calculations. The scheme includes parameters for tropical and polar relaxation times, and for a temporal dependence, and these can readily be used to modify the structure of the stratosphere, and in particular the strength of the polar vortex strength.

In agreement with *Gerber and Polvani* [2009], the stronger the polar vortex is in the relaxation temperature T_e, the fewer SSWs occur, and the stronger orographic forcing (higher mountains), the more SSWs are produced. In addition to confirming these previous findings, we have extended the parameter range to include variations of the relaxation time, noting that these can be modified in the low- and high-latitudes independently.

As a general rule, we found that the longer the relaxation time (i.e., the weaker the damping) the more frequent are SSWs. Concerning differences between the low- and high-latitude damping rates, we found that whichever is weaker (longer time scales) tends to dominate the sensitivity of the SSW frequency with respect to a fractional change in either of the two damping rates. In particular, with the relaxation time in the low latitudes, denoted τ_t, fixed at a small value of 20 days, changing the relaxation time at high latitudes, denoted τ_p, has a big impact on the frequency of SSWs. When fixing τ_t to a large value of 40 days, the impact of changing τ_p is considerably diminished. The same can be said for the inverse argument: Fixing τ_p to a short value, changing τ_t has a large impact on SSW frequency, whereas that impact decreases when τ_p is chosen to have a large value. Given the large uncertainties in radiative damping rates of the real atmosphere and the large spread for relaxation times applied to various Newtonian cooling schemes in the literature, the here presented results can give guidance to the consequences of choosing a given time scale. This includes the effects of including/excluding a latitudinal gradient in relaxation time, as suggested by radiative considerations [*Kiehl and Solomon*, 1986; *Newman and Rosenfield*, 1997]. Previous findings from *Jucker et al.* [2013] suggest that for realistic simulations of Earth's atmosphere, the high-latitude relaxation time should be rather short (around 20 d at 100 hPa), whereas the low-latitude relaxation time should be considerably longer (around 40 d at 100 hPa).

Furthermore, we have studied the correlations between the SSW frequency and the climatological variables that can be obtained directly from reanalysis or other numerical models. Above the tropopause, polar cap averaged zonal mean zonal wind climatology is strongly anticorrelated to the occurrence rate of SSWs throughout the stratosphere. Other strong correlations in the stratosphere (though much more localized in the vertical) can be found with the polar cap zonal mean temperature climatology between about 150 hPa and 30 hPa, extratropical eddy heat flux at 100 hPa, and there is a narrow peak of anticorrelation with eddy momentum flux around 30 hPa. Our studies indicate that the choice of 10 hPa for SSW detection is rather arbitrary, and 30 hPa more significant. The difference in temperature between the midlatitudes and polar cap is the only quantity to show strong (anti)correlation in the troposphere, indicating that baroclinicity in the troposphere plays an important role for the occurrence rate of SSWs.

Appendix A: Analytic Profile Description

The modifications to the original spectral dynamical core, along with Matlab scripts for automatically generating the here discussed relaxation profiles are available online at https://github.com/mjucker/JFV-strat. Figure A1 shows the analytical profiles of T_e (a) and τ (b) for simulation 3, where the strength of the polar vortex roughly corresponds to a late Northern Hemisphere winter configuration of *Jucker et al.* [2013].

A1. Temperature

The vertical profile of T_e is based on the radiatively found T_e over the equator. It is approximated with two polynomials, one above and one below p_1 =1 hPa:

$$k = \ln(p/p_0) \tag{A1}$$

$$\mathcal{P}_1(p) = -0.537k^4 - 9.65k^3 - 60.6k^2 - 174k + 19.8 \tag{A2}$$

$$\mathcal{P}_2(p) = 0.668k^3 + 22.3k^2 + 248k + 1160 \tag{A3}$$

$$T_e^{\mathrm{EQ}}(p) = \begin{cases} \max\left(T_T, \mathcal{P}_1(p)\right) & , p \geq p_1 \\ \max\left(\mathcal{P}_1(p), \mathcal{P}_2\right) & , p < p_1. \end{cases} \tag{A4}$$

The variation in latitude is modeled starting from the equinoxes, with a profile linear in ln p and a 4 order polynomial in latitude (and thus north-south symmetric). The pressure of the upper limit of the Held-Suarez configuration is denoted by p_t =100 hPa.

$$\mathcal{P}_3(\varphi) = -1.96 \times 10^{-9}\varphi^4 - 1.15 \times 10^{-5}\varphi^2 + 1 \tag{A5}$$

$$l = \ln(p/p_t)/\ln(p_1/p_t) \tag{A6}$$

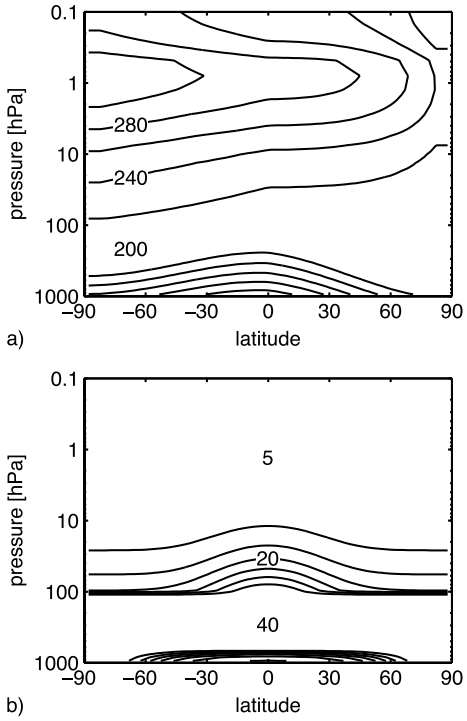

Figure A1. Example of analytically described (a) T_e and (b) τ. This example corresponds to the setup of simulation 3, with a weak polar vortex and high-latitude relaxation times that are shorter than over the equator. Numbers in the figures denote (Figure A1a) T_e values in Kelvin and (Figure A1b) τ values in days.

$$\mathcal{P}_4(\varphi,p)=\begin{cases}1 & ,p\geq p_t\\ \left(\mathcal{P}_3(\varphi)-1\right)l+1 & ,p_t>p>p_1\\ \mathcal{P}_3(\varphi) & ,p\leq p_1,\end{cases} \tag{A7}$$

where the latitude φ is in units of degrees in the polynomial $\mathcal{P}_3$ of equation (A5).

The seasonal amplitudes of T_e in the Northern and Southern Hemispheres have the same mathematical description but can be chosen to differ. Input parameters are p_0 =1000 hPa and $A^{0,1}_{\mathrm{NH,SH}}$. For each hemisphere, denoted NH for the Northern Hemisphere and SH for the Southern Hemisphere, a lower stratospheric amplitude $A^0_{\mathrm{NH,SH}}=A_{\mathrm{NH,SH}}(p=p_t)$ and an upper stratospheric amplitude $A^1_{\mathrm{NH,SH}}=A_{\mathrm{NH,SH}}(p=p_1)$ can be chosen. These are the amplitudes for the respective winter solstices. For the summer solstices, a different amplitude A_s serves as input parameter and is the same in the northern and summer hemispheres.

$$\delta p=\ln(p_1/p_0)-\ln(p_t/p_0) \tag{A8}$$

$$A_W(\varphi,p)=-\frac{|\varphi|}{90}\begin{cases}\frac{A^1_{\mathrm{NH}}-A^0_{\mathrm{NH}}}{\delta p}\ln(p/p_t)+A^0_{\mathrm{NH}} & ,\varphi\geq 0\\ \frac{A^1_{\mathrm{SH}}-A^0_{\mathrm{SH}}}{\delta p}\ln(p/p_t)+A^0_{\mathrm{SH}} & ,\varphi<0\end{cases} \tag{A9}$$

$$A_S(\varphi,p)=-\frac{|\varphi|}{90}\left(\frac{A_s}{\delta p}\ln(p/p_t)+A_s\right) \tag{A10}$$

$$A(\varphi,p<p_1)=A(p_1). \tag{A11}$$

Finally, temporal dependence is introduced with two cosines, one centered around day 0/365 and the other around day 182.5, and the variable d denotes the day of the climatological year. Note here that these choices set Northern Hemisphere winter solstice to 31 December and Southern Hemisphere winter solstice to 1 July. This can easily be adapted if necessary.

$$D(\varphi,d)=\begin{cases}\cos(2\pi d/365) & ,\varphi\geq 0\\ \cos(2\pi(d-182.5)/365) & ,\varphi<0\end{cases}, \tag{A12}$$

and all terms are put together to obtain a latitude-pressure-time dependent $T_e^{\mathrm{strat}}(\varphi,p,d)$:

$$T_e^{\mathrm{strat}}(\varphi,p,d)=T_e^{\mathrm{EQ}}(p)\mathcal{P}_4(\varphi,p)+\begin{cases}A_W(\varphi,p)D(\varphi,d) & ,D(\varphi,d)\geq 0\\ \left[A_S(\varphi,p)-T_e^{\mathrm{EQ}}(p)(1-\mathcal{P}_4(\varphi,p))\right]D(\varphi,d) & ,D(\varphi,d)<0\end{cases} \tag{A13}$$

$$T_e^{\mathrm{strat}}(\varphi>\varphi_N,p,d)=T_e^{\mathrm{strat}}(\varphi_N,p,d) \tag{A14}$$

$$T_e^{\mathrm{strat}}(\varphi>\varphi_S,p,d)=T_e^{\mathrm{strat}}(\varphi_S,p,d). \tag{A15}$$

Table A1 summarizes the free parameters and their default values for describing the T_e profile. The defaults are based on the best approximation to the radiatively determined January setup of *Jucker et al.* [2013].

Table A1. Input Parameters Defining the Analytic Profile for the Relaxation Temperature T_e

Name	Meaning	Default
p_0	surface pressure	1000 hPa
p_t	lower stratosphere reference pressure	100 hPa
p_1	upper stratosphere reference pressure	1 hPa
T_T	minimum temperature below p_t	200 K
A^0_{NH}	amplitude at $p = p_t$, 90°N (winter)	15 K
A^1_{NH}	amplitude at $p = p_1$, 90°N (winter)	45 K
A^0_{SH}	amplitude at $p = p_t$, 90°S (winter)	25 K
A^1_{SH}	amplitude at $p = p_1$, 90°S (winter)	60 K
A_s	amplitude at $p = p_1$, Summer Pole	15 K

A2. Relaxation Time

The relaxation time has two main contributions. One is an equator-to-pole gradient, which can be a function of time. The parameters defining this meridional gradient are the relaxation time over the southern and northern poles at $p = p_t$, denoted $\tau_p^S(d)$ and $\tau_p^N(d)$, respectively, and the width $\Delta\varphi$ of a Gaussian placed over the tropics. The relaxation time at the pressure level $p = p_t$ is then determined by

$$\tau_{p_t}(\varphi, d) = \begin{cases} \tau_p^S(d) + (\tau_t(d) - \tau_p^S(d)) \exp[-(\varphi/\Delta\varphi)^2] & , \varphi < 0 \\ \tau_p^N(d) + (\tau_t(d) - \tau_p^N(d)) \exp[-(\varphi/\Delta\varphi)^2] & , \varphi \geq 0. \end{cases} \tag{A16}$$

The second contribution is a polynomial decrease with height from p_t, where the relaxation time is defined by (A16), to the top of the atmosphere. Additional input parameter defining this profile is the minimum relaxation time at the top of the atmosphere τ_m. The profile is then determined by

$$k = \ln(p/p_0) \tag{A17}$$

$$\mathcal{P}_p(p) = 0.045k^4 + 1.38k^3 + 15.9k^2 + 81.6k + 162 \tag{A18}$$

$$\mathcal{P}_p(p < 0.1)\,\mathrm{hPa}) = \mathcal{P}_p(p = 0.1\,\mathrm{hPa}) \tag{A19}$$

$$\mathcal{P}_n(p) = \frac{\mathcal{P}_p(p) - \min(\mathcal{P}_p(p))}{\mathcal{P}_p(p_t) - \min(\mathcal{P}_p(p))}. \tag{A20}$$

Finally, putting together the profiles in pressure and latitude yields the complete relaxation time structure

$$\tau^{\mathrm{strat}}(\varphi, p, d) = \left(\tau_{p_t}(\varphi, d) - \tau_m\right) \mathcal{P}_n(p, d) + \tau_m. \tag{A21}$$

Note that the radiatively found τ profiles of *Jucker et al.* [2013] include a small correction over the poles, with a small increase in relaxation time in the cold polar vortex (longer time scales for lower temperatures). We did not include this effect, as it is a small correction and did not yield significantly different results when included in the analytical profiles or excluded in the radiative profiles. Table A2 summarizes the free parameters for the τ profile and its default values.

Table A2. Input Parameters Defining the Analytic Profile for the Relaxation Time τ

Parameter	Meaning	Default
p_0	surface pressure	1000 hPa
p_t	lower stratosphere reference pressure	100 hPa
τ_t	relaxation time over tropics at $p = p_t$	40 d
τ_m	shortest relaxation time over tropics	5 d
$\Delta\phi$	meridional width around tropics	30°
τ_p^S	relaxation time over South Pole	20 d
τ_p^N	relaxation time over North Pole	20 d

Acknowledgments
This work was supported by the National Science Foundation under grant AGS-1144302, and M.J. is supported by the Swiss National Science Foundation. Data are available upon author request.

References

Baldwin, M. P., and T. J. Dunkerton (2001), Stratospheric harbingers of anomalous weather regimes, *Science*, *294*(5542), 581–584, doi:10.1126/science.1063315.
Baldwin, M. P., D. W. Thompson, E. F. Shuckburgh, W. A. Norton, and N. P. Gillett (2003), Atmospheric science. Weather from the stratosphere?, *Science*, *301*(5631), 317–319, doi:10.1126/science.1085688.
Charlton, A. J., and L. M. Polvani (2007), A new look at stratospheric sudden warmings. Part I: Climatology and modeling benchmarks, *J. Clim.*, *20*(3), 449–469, doi:10.1175/JCLI3996.1.
Charlton-Perez, A. J., and A. O'Neill (2010), On the sensitivity of annular mode dynamics to stratospheric radiative time scales, *J. Clim.*, *23*(2), 476–484, doi:10.1175/2009JCLI2995.1.
Dickinson, R. E. (1973), Method of parameterization for infrared cooling between altitudes of 30 and 70 kilometers, *J. Geophys. Res.*, *78*(21), 4451–4457.
Fels, S. B. (1982), A parametrization of scale-dependent radiative damping rates in the middle atmosphere, *J. Atmos. Sci.*, *39*, 1141–1152.
Gerber, E. P., and L. M. Polvani (2009), Stratosphere-troposphere coupling in a relatively simple AGCM: The importance of stratospheric variability, *J. Clim.*, *22*(8), 1920–1933.
Gerber, E. P., et al. (2012), Assessing and understanding the impact of stratospheric dynamics and variability on the Earth system, *Bull. Am. Meteorol. Soc.*, *93*(6), 845–859, doi:10.1175/BAMS-D-11-00145.1.
Ghazi, A., P.-H. Wang, and M. P. McCormick (1985), A study on radiative damping of planetary waves utilizing stratospheric observations, *J. Atmos. Sci.*, *42*(19), 2032–2042, doi:10.1175/1520-0469(1985)042<2032:ASORDO>2.0.CO;2.
Gómez-Escolar, M., S. Fueglistaler, N. Calvo, and D. Barriopedro (2012), Changes in polar stratospheric temperature climatology in relation to stratospheric sudden warming occurrence, *Geophys. Res. Lett.*, *39*, L22802, doi:10.1029/2012GL053632.
Hartmann, D. L., J. R. Holton, and Q. Fu (2001), The heat balance of the tropical tropopause, cirrus, and stratospheric dehydration, *Geophys. Res. Lett.*, *28*(10), 1969–1972, doi:10.1029/2000GL012833.
Hitchcock, P., T. G. Shepherd, M. Taguchi, S. Yoden, and S. Noguchi (2013), Lower-stratospheric radiative damping and polar-night jet oscillation events, *J. Atmos. Sci.*, *70*(5), 1391–1408, doi:10.1175/JAS-D-12-0193.1.
Holton, J. J. R., P. H. P. Haynes, M. E. M. McIntyre, A. R. Douglass, R. B. R. Rood, L. L. Pfister, and A. Douglas (1995), Stratosphere-troposphere exchange, *Rev. Geophys.*, *33*(4), 403–440, doi:10.1029/95RG02097.
Jucker, M., S. Fueglistaler, and G. K. Vallis (2013), Maintenance of the stratospheric structure in an idealized general circulation model, *J. Atmos. Sci.*, *70*(11), 3341–3358, doi:10.1175/JAS-D-12-0305.1.
Kiehl, J. T., and S. Solomon (1986), On the radiative balance of the stratosphere, *J. Atmos. Sci.*, *43*(14), 1525–1534, doi:10.1175/1520-0469(1986)043<1525:OTRBOT>2.0.CO;2.
Kodera, K. (2006), Influence of stratospheric sudden warming on the equatorial troposphere, *Geophys. Res. Lett.*, *33*, L06804, doi:10.1029/2005GL024510.
Kouker, W., and G. Brasseur (1986), Transport of atmospheric tracers by planetary waves during a winter stratospheric warming event: A three-dimensional model simulation, *J. Geophys. Res.*, *91*(D12), 13,167–13,185, doi:10.1029/JD091iD12p13167.
Kushner, P. J., and L. M. Polvani (2004), Stratosphere-troposphere coupling in a relatively simple AGCM: The role of eddies, *J. Clim.*, *17*(3), 629–639, doi:10.1175/1520-0442(2004)017<0629:SCIARS>2.0.CO;2.
Limpasuvan, V., D. W. J. Thompson, and D. L. Hartmann (2004), The life cycle of the Northern Hemisphere sudden stratospheric warmings, *J. Clim.*, *17*(13), 2584–2596, doi:10.1175/1520-0442(2004)017<2584:TLCOTN>2.0.CO;2.
Mitchell, D. M., L. J. Gray, J. Anstey, M. P. Baldwin, and A. J. Charlton-Perez (2013), The influence of stratospheric vortex displacements and splits on surface climate, *J. Clim.*, *26*(8), 2668–2682, doi:10.1175/JCLI-D-12-00030.1.
Miyakoda, K., R. F. Strickler, and G. D. Hembree (1970), Numerical simulation of the breakdown of a polar-night vortex in the stratosphere, *J. Atmos. Sci.*, *27*(1), 139–154, doi:10.1175/1520-0469(1970)027<0139:NSOTBO>2.0.CO;2.
Nakagawa, K. I., and K. Yamazaki (2006), What kind of stratospheric sudden warming propagates to the troposphere?, *Geophys. Res. Lett.*, *33*, L04801, doi:10.1029/2005GL024784.
Newman, P. A., and J. E. Rosenfield (1997), Stratospheric thermal damping times, *Geophys. Res. Lett.*, *24*(4), 433–436, doi:10.1029/96GL03720.
Polvani, L. M., and P. J. Kushner (2002), Tropospheric response to stratospheric perturbations in a relatively simple general circulation model, *Geophys. Res. Lett.*, *29*(7), 18-1–18-4, doi:10.1029/2001GL014284.
Polvani, L. M., and D. W. Waugh (2004), Upward wave activity flux as a precursor to extreme stratospheric events and subsequent anomalous surface weather regimes, *J. Clim.*, *17*(18), 3548–3554, doi:10.1175/1520-0442(2004)017<3548:UWAFAA>2.0.CO;2.
Ramanathan, V., E. J. Pitcher, R. C. Malone, and M. L. Blackmon (1983), The response of a spectral general circulation model to refinements in radiative processes, *J. Atmos. Sci.*, *40*(3), 605–630, doi:10.1175/1520-0469(1983)040<0605:TROASG>2.0.CO;2.
Sigmond, M., J. F. Scinocca, V. V. Kharin, and T. G. Shepherd (2013), Enhanced seasonal forecast skill following stratospheric sudden warmings, *Nat. Geosci.*, *6*(2), 98–102, doi:10.1038/ngeo1698.
Yoden, S., T. Yamaga, S. Pawson, and U. Langematz (1999), A composite analysis of the stratospheric sudden warmings simulated in a perpetual january integration of the Berlin TSM GCM, *J. Meteorol. Soc. Jpn.*, *77*(2), 431–445.

Erratum

In the originally published version of this article, typos were present in Equation A6, Equation A7, and Table A1. These errors have since been corrected and this version may be considered the authoritative version of record.